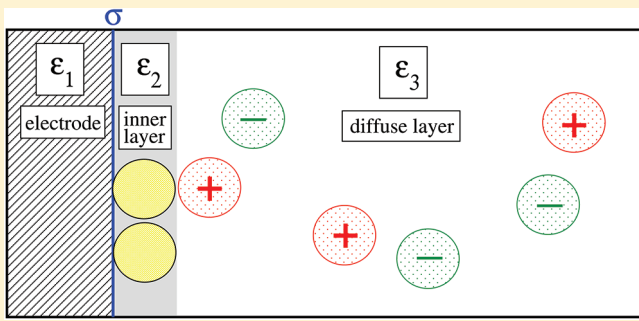


Simulation of an Electrical Double Layer Model with a Low Dielectric Layer between the Electrode and the Electrolyte

Tímea Nagy,[†] Douglas Henderson,[‡] and Dezső Boda^{*,†,‡}[†]Department of Physical Chemistry, University of Pannonia, P.O. Box 158, H-8201 Veszprém, Hungary[‡]Department of Chemistry and Biochemistry, Brigham Young University, Provo, Utah 84602, United States

ABSTRACT: We report Monte Carlo simulation results for double layers of 1:1 and 2:1 electrolytes near an electrode with an inner layer that has a dielectric constant, ϵ_2 , smaller than that of the electrolyte, ϵ_3 . The electrolyte is modeled in the implicit solvent framework (primitive model), while the electrode is a metal electrode in this study ($\epsilon_1 \rightarrow \infty$). The charged hard sphere ions are not allowed to enter into the inner layer. We show that the capacitance of the inner layer is $C_\delta = \epsilon_0(\epsilon_2 + \epsilon_3)/2\delta$, where δ is the thickness of the inner layer. This result is different from that obtained from solutions of the Poisson–Boltzmann equation ($\epsilon_0\epsilon_2/\delta$), indicating that interpretation of experimental data with a fitted ϵ_2 dielectric constant of the inner layer must be done using a different equation. We also show that the properties of the diffuse layer are not independent of the value of ϵ_2 , which is a usual assumption of the Poisson–Boltzmann theory. This is mainly because the repulsive image charges repel both the counterions and the co-ions, while the electrode charge attracts the counterions and repels the co-ions.



INTRODUCTION

The electrical double layer (DL) is commonly modeled as an interface of an implicit solvent electrolyte and a flat electrode carrying a constant surface charge. In the solution of Gouy¹ and Chapman² for the Poisson–Boltzmann (PB) equations, the ions are modeled as point charges (apart from a possible nonzero distance of closest approach (DCA) to the electrode), while in more developed statistical mechanical theories and simulations, the ions are modeled as charged hard spheres (the primitive model (PM) of electrolytes).

The electrode is usually modeled as a dielectric continuum with the same dielectric constant as the electrolyte. In such a system, the dielectric is homogeneous (the dielectric constant is the same everywhere), and the forces are pairwise additive, which makes the application of statistical mechanical theories using pair correlation functions^{3–7} straightforward.

When the electrode has a dielectric constant (a value approaching infinity, $\epsilon_1 \rightarrow \infty$, for example, mimics a metal electrode) different from that of the electrolyte (ϵ_3), a dielectric boundary appears in the system. Polarization charges are induced by the ions on this boundary, and the forces are no longer pairwise additive. Different methods cope with this problem in different ways. PB theories^{8–11} assume that the dielectric constant of the electrode has no effect on the ionic charge profile (and, consequently, on the potential profile) in the diffuse layer. Simulations can deal with this situation straightforwardly with the application of image charges.^{12–24} It was shown by Torrie and Valleau^{13,14} that the assumption of PB theories is not valid, especially for electrolytes containing multivalent ions.

Theories have problems in the presence of dielectric boundaries because most of these theories use pair-correlation functions.^{4,13,18,25–34} The proper treatment of a dielectric interface requires multibody interactions (three particles: a pair of ions and the surface at a minimum). A simple approach that uses a screened self-image interaction has been proposed by Onsager and Samara.³⁵ This approach is really too crude, although it is better than nothing. Some approaches that include multibody correlation functions are those of Carnie and Chan,²⁵ Plischke and Henderson,⁵ Kjellander and Marcelja,²⁶ Croxton et al.,¹² Vertenstein and Ronis,²⁷ and Outhwaite and Bhuiyan.⁴ However, only the Outhwaite–Bhuiyan approach, which they call the modified PB or MPB theory, has been used extensively. The MPB theory is reasonably accurate. However, the extent to which the MPB theory can be adapted to include an intermediate dielectric layer, such as that considered here, is uncertain. Recently, Gillespie³⁶ has proposed a density functional theory that is a promising tool with which geometries beyond the simple flat dielectric boundary could be studied.

No matter which method or model is used, however, to bring results into agreement with experiments, it is necessary^{37–41}—or at least sufficient—to postulate an interfacial region or inner layer (also called a Helmholtz or Stern layer) of some thickness δ in which the dielectric coefficient (ϵ_2) is smaller than that of the bulk electrolyte (ϵ_3). In PB theories, it is an everyday practice to

Received: July 5, 2011

Revised: August 5, 2011

Published: August 17, 2011

write the capacitance of the DL in the form:

$$\frac{1}{C} = \frac{1}{C_\delta} + \frac{1}{C_{\text{diff}}} \quad (1)$$

where C_δ and C_{diff} are the capacitances of the inner layer and the diffuse layer, respectively. The solution of the PB theory gives that $C_{\text{diff}} \sim c^{1/2}$, where c is the concentration. Because the inner layer is an ion-free region, its capacitance is $C_\delta^{-1} = (\epsilon_0 \epsilon_3 / \delta)^{-1}$ for the case when the dielectric constant is the same everywhere ($\epsilon_1 = \epsilon_2 = \epsilon_3$).

Inspired by the PB theory, Parsons and Zobel³⁸ suggested plotting $1/C$ as a function of $1/C_{\text{diff}}$ or, alternatively, as a function of $1/c^{1/2}$ (Parsons–Zobel plot). The result is a nearly linear function whose slope is well described by the PB theory at small concentrations. Deviations occur at large concentrations. The y -intercept of a linear curve fitted on the experimental data (for an aqueous solution of NaH_2PO_4 at 25 °C near a hanging mercury electrode), however, was quite different from the $C_\delta^{-1} = (\epsilon_0 \epsilon_3 / \delta)^{-1}$ value provided by the PB theory. To shift the linear curve along the ordinate, a capacitance that is connected in series with the diffuse layer capacitance must be introduced. A possible choice is to assign this capacitance to an inner layer and to scale the inner layer capacitance by writing $C_\delta^{-1} = (\epsilon_0 \epsilon_2 / \delta)^{-1}$, where ϵ_2 is identified as the dielectric constant of the inner layer.

This value appeared in formal solutions of the PB theory (see, for example, eq 5 of the paper of Andreu et al.⁹). In this work, we derive a different solution for the inner layer capacitance for the case when the electrode is a metal electrode. Thus, our work places modeling of the inner layer into a different perspective.

The inner layer can be visualized as a compact layer of highly ordered water molecules at the electrode (Figure 1). Due to dielectric saturation, the dielectric constant in this layer is smaller than in the electrolyte, where water molecules are more irregularly oriented.

This geometry (called slab geometry from now on) is even more complex than the geometry without the inner layer. The image charge approach cannot be used, because an infinite number of image charges (or, equivalently, a series expansion) is needed to treat the electrostatic problem. The only simulation study, to our knowledge, on this geometry was published by us some years ago.²⁹ It became possible because a numerical method, the induced charge computation (ICC) method^{42,43} was developed to solve Poisson's equation for arbitrary dielectric boundaries in a simulation. In that paper, we have also published and tested an extension of the PB theory due to Onsager and Samara.³⁵

Our earlier study, however, considered only zero surface charges due to technical problems. This technical problem (the balance of induced charges outside the central simulation cell) is solved in this work. Therefore, we are in the position to publish results for nonzero electrode charges and capacitances in this paper. One of the goals of this paper is to present this methodology in detail. Due to the complexity of the electrostatic problem, understanding these details is necessary to elucidate the results.

The other goal of this paper is to study the behavior of the DL in the presence of a low dielectric inner layer with Monte Carlo (MC) simulations. In particular, it is our purpose to test the assumption of PB theories that the presence of the inner layer has no effect on the behavior of the diffuse layer. Furthermore, PB theories assume that the diffuse layer capacitance, C_{diff} , is independent of the value of ϵ_2 . We also show in this paper that

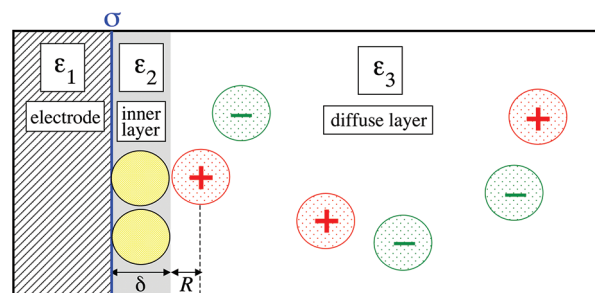


Figure 1. Illustration of the geometry. A low dielectric layer (ϵ_2) of water molecules (inner layer) is placed between the electrode ($\epsilon_1 \rightarrow \infty$) and the electrolyte ($\epsilon_3 = 80$). The width of the inner layer is $\delta = 3 \text{ \AA}$. The ions are not allowed to enter the inner layer in this study: the $\epsilon_2|\epsilon_3$ boundary acts as a hard wall for the hard sphere ions. The contact distance of the ion centers from the electrode is $\delta + R$, where $R = 1.5 \text{ \AA}$ is the radius of the ions in the RPM. A constant σ surface charge is placed on the surface of the electrode at the $\epsilon_1|\epsilon_2$ boundary.

this assumption is not valid and especially erroneous for 2:1 electrolytes.

Ions are excluded from the inner layer in this work. This might be a reasonable assumption at zero and low electrode charges, but it fails for large electrode charges that can attract the counterions into the inner layer. Simulations where charged hard spheres (spheres with point charges in their centers) can cross the dielectric boundary between the inner layer and the bulk electrolyte are problematic because the energy diverges as a point charge approaches a dielectric boundary. We have developed a solution for this problem,⁴⁴ but have not yet incorporated this into a DL simulation. Simulations where ions can enter the inner layer will be published subsequently.

■ MODEL AND METHOD

Model of the Double Layer. Our DL model (Figure 1) is based on the PM of electrolytes, where the ions are modeled as point charges in the centers of hard spheres (the interaction energy will be given in subsection “Computation of the energy”), while the solvent is represented as a dielectric continuum of dielectric constant ϵ_3 . In this work, we use the restricted PM (RPM), in which the radii of the cations and anions are equal, R .

The electrolyte is near a charged polarizable electrode, which is modeled by a continuum of a dielectric constant ϵ_1 (see Figure 1). In this work, we consider perfectly polarizable metal electrodes, where the dielectric constant is infinitely large: $\epsilon_1 \rightarrow \infty$. In this case, any external charge is spread on the surface of the electrode in the region of dielectric constant ϵ_2 . We use a constant surface charge σ . The surface of the electrode is at the origin $x = 0$.

An inner layer of a dielectric constant ϵ_2 and thickness $\delta = 3 \text{ \AA}$ is applied at the electrode. Ions are excluded from this region, so the dielectric boundary at $x = \delta$ acts as a hard wall for the hard sphere ions. This means that the DCA of the ions to the electrode is $\delta + R$.

The simulation cell is closed by a hard wall at $x = H$. This wall can also be charged (σ_H), but this has no consequence on the structure of the DL at the left electrode as soon as H is large enough so the DLs at $x = 0$ and $x = H$ are independent.

Periodic boundary conditions are applied in the y,z dimensions. This means that the space is filled with the periodic images

of the central simulation cell (of width L) in the y and z dimensions. When interactions between two charges are considered, the distance between a charge and the closest image is used (minimum image convention). This is true no matter whether the charges are free charges or induced charges.

Computation of Induced Charges on the Dielectric Boundaries. The three dielectric regions form a slab geometry, where the ε_2 slab is confined between the ε_1 and ε_3 regions. Two dielectric boundaries are formed: an $\varepsilon_1|\varepsilon_2$ boundary at $x = 0$ (indexed by 1) and an $\varepsilon_2|\varepsilon_3$ boundary at $x = \delta$ (indexed by 2).

The induced charges on these dielectric boundaries can be calculated by the ICC method.^{42,43} It is based on an integral equation using the induced charge as an unknown variable instead of partial differential equations (the Poisson's equation with boundary conditions) using the electrical potential as an unknown variable. The ICC equation is

$$\begin{aligned} \bar{\varepsilon}(\mathbf{s}) h(\mathbf{s}) + \frac{1}{4\pi} \int_{\mathcal{B}} d\mathbf{s}' h(\mathbf{s}') \frac{(\mathbf{s} - \mathbf{s}') \cdot \mathbf{n}(\mathbf{s})}{|\mathbf{s} - \mathbf{s}'|^3} \\ = -\frac{1}{4\pi} \sum_k \frac{q_k}{\varepsilon(\mathbf{r}_k)} \frac{(\mathbf{s} - \mathbf{r}_k) \cdot \mathbf{n}(\mathbf{s})}{|\mathbf{s} - \mathbf{r}_k|^3} \end{aligned} \quad (2)$$

where \mathcal{B} is the entire dielectric boundary in the system, $h(\mathbf{s})$ is the induced charge, $\bar{\varepsilon}(\mathbf{s})$ and $\Delta\varepsilon(\mathbf{s})$ are the mean and difference of the dielectric coefficients on the two sides of the boundary at \mathbf{s} , and $\mathbf{n}(\mathbf{s})$ is the normal vector of the surface at point \mathbf{s} . The right-hand side of the equation is proportional to the normal electric field produced by the source point charges q_k in the system. The point charges are in positions \mathbf{r}_k in a region of dielectric coefficient $\varepsilon(\mathbf{r}_k)$ (ε_3 , in this work). Both $\mathbf{s} - \mathbf{s}'$ and $\mathbf{s} - \mathbf{r}_k$ are minimum image vectors.

The solution of this equation is obtained numerically by dividing the whole surface \mathcal{B} into surface elements \mathcal{B}_α (tiles). Assuming that $h_\alpha = h(\mathbf{s}_\alpha)$ is constant on the α th tile, where \mathbf{s}_α is the center of the α th tile, the equation can be written for \mathbf{s}_α as

$$\begin{aligned} \sum_\beta h_\beta \left[\frac{\bar{\varepsilon}(\mathbf{s}_\alpha)}{\Delta\varepsilon(\mathbf{s}_\alpha)} \delta_{\alpha\beta} + \frac{1}{4\pi} I_{\alpha\beta} \right] \\ = -\frac{1}{4\pi} \sum_k \frac{q_k}{\varepsilon(\mathbf{r}_k)} \frac{(\mathbf{s}_\alpha - \mathbf{r}_k) \cdot \mathbf{n}(\mathbf{s}_\alpha)}{|\mathbf{s}_\alpha - \mathbf{r}_k|^3} \end{aligned} \quad (3)$$

where the integral

$$I_{\alpha\beta} = \int_{\mathcal{B}_\beta} d\mathbf{s}' \frac{(\mathbf{s}_\alpha - \mathbf{s}') \cdot \mathbf{n}(\mathbf{s}_\alpha)}{|\mathbf{s}_\alpha - \mathbf{s}'|^3} \quad (4)$$

expresses the mutual polarization between tiles α and β . This system of linear equations can be expressed as a matrix equation

$$\mathbf{Ah} = \mathbf{c} \quad (5)$$

where matrix \mathbf{A} is defined by the expression in brackets in eq 3. The vector \mathbf{h} contains the surface charges at the tile centers, while vector \mathbf{c} contains the direct effect of the source charges. The source charges are the ionic charges or electrode charges in this work. The vector \mathbf{c} changes as ions move in the simulation; the induced charge can be obtained from an LU backsubstitution in every simulation step. The filling of the matrix and its LU decomposition are very time-consuming processes, but they can be done once at the beginning of the simulation because the geometry of the dielectric boundaries does not change in the simulation.

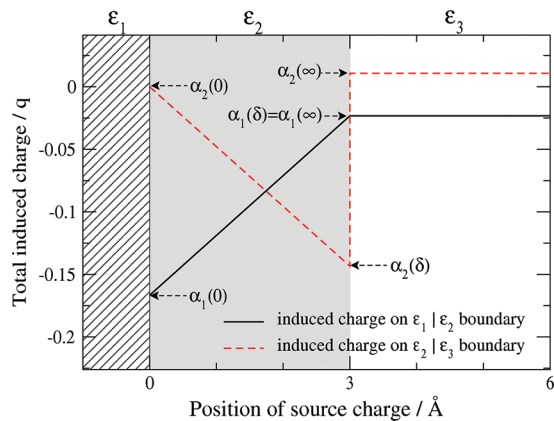


Figure 2. Illustration of the sum rule for the total induced charge for the slab geometry (see eq 7). The total charges induced on the $\varepsilon_1|\varepsilon_2$ and $\varepsilon_2|\varepsilon_3$ boundaries by a source charge q are plotted as functions of the position of the source charge. The dielectric constants for the case plotted in the figure are $\varepsilon_1 \rightarrow \infty$, $\varepsilon_2 = 6$, $\varepsilon_3 = 80$ (see eq 8).

In the DL geometry, the dielectric boundary extends to infinity in the y and z dimensions. In the ICC method, however, the dielectric boundaries are necessarily finite: they are $L \times L$ squares at $x = 0$ and $x = \delta$. Let us denote these squares by \mathcal{L}_1 and \mathcal{L}_2 . The induced charges that are outside these squares are missing from the calculations causing serious charge-neutrality problems. These charges, therefore, should be taken into account and balanced in the energy calculation.

Sum Rule for the Induced Charges. A straightforward method to solve this problem is to compute the total induced charges on both finite discretized dielectric boundaries,

$$h_i^{\text{tot}} = \sum_{\alpha \in \mathcal{L}_i} h_\alpha a_\alpha \quad (6)$$

where $i = 1$ or 2 and a_α is the area of the α th tile. Then, we deduct them from the values that they should have for the infinite boundaries h_1^{sm} and h_2^{sm} . This way, we obtain the missing (or excess) charges that we should balance: $\Delta h_1^{\text{tot}} = h_1^{\text{sm}} - h_1^{\text{tot}}$ and $\Delta h_2^{\text{tot}} = h_2^{\text{sm}} - h_2^{\text{tot}}$. The method with which we balance them will be given in the next subsection. Here, we focus on the calculation of h_i^{sm} .

The superscript "sm" refers to the term "sum rule". This means that the total charge on the dielectric boundaries induced by a source charge in a given position can be computed from integral laws of electrostatics (Gauss' law). The induced charges computed with a numerical method should obey these "sum rules" with a good accuracy.⁴³ The "sum rule" for the slab geometry gives the total polarization charges on boundaries \mathcal{L}_1 and \mathcal{L}_2 induced by a source charge. These charges, $h_1^{\text{sm}}(x)$ and $h_2^{\text{sm}}(x)$, depend on the position x of the q source charge. Let us denote the total charge on boundary i induced by a unit charge at position x with $\alpha_i(x)$. The total charge induced by a charge q on boundary i then is $h_i^{\text{sm}}(x) = \alpha_i(x)q$.

We show results only for $x > 0$, because the solution for $x < 0$ is analogous to the solution for $x > \delta$. Figure 2 shows that the induced charge on the dielectric boundaries is constant if the position of the source charge is $x > \delta$ no matter where is the source charge in the ε_3 region. The corresponding values will be denoted by $\alpha_1(\infty)$ and $\alpha_2(\infty)$ for the two dielectric boundaries.

When the source charge is in the ε_2 region (the inner layer), the total induced charge varies linearly between two limiting

values. These limiting values are the total induced charges induced by a unit charge that is (1) at the right-hand side of the $\varepsilon_1|\varepsilon_2$ boundary infinitely close to it, and (2) at the left-hand side of the $\varepsilon_2|\varepsilon_3$ boundary infinitely close to it. These values will be denoted by $\alpha_i(0)$ and $\alpha_i(\delta)$, respectively. The sum rules are given by the following equations:

$$\begin{aligned}\alpha_1(0) &= -\frac{\varepsilon_1 - \varepsilon_2}{\varepsilon_2(\varepsilon_1 + \varepsilon_2)} \\ \alpha_1(\delta) &= \alpha_1(\infty) = -\frac{2(\varepsilon_1 - \varepsilon_2)}{(\varepsilon_1 + \varepsilon_2)(\varepsilon_3 + \varepsilon_2)} \\ \alpha_2(0) &= -\frac{2(\varepsilon_3 - \varepsilon_2)}{(\varepsilon_1 + \varepsilon_2)(\varepsilon_3 + \varepsilon_2)} \\ \alpha_2(\delta) &= -\frac{\varepsilon_3 - \varepsilon_2}{\varepsilon_2(\varepsilon_3 + \varepsilon_2)} \\ \alpha_2(\infty) &= \frac{\varepsilon_3 - \varepsilon_2}{\varepsilon_3(\varepsilon_3 + \varepsilon_2)}\end{aligned}\quad (7)$$

For the special case when $\varepsilon_1 \rightarrow \infty$, the first three of these equations reduce to

$$\begin{aligned}\alpha_1(0) &= -\frac{1}{\varepsilon_2} \\ \alpha_1(\delta) &= \alpha_1(\infty) = -\frac{2}{\varepsilon_3 + \varepsilon_2} \\ \alpha_2(0) &= 0\end{aligned}\quad (8)$$

while the last two equations are unchanged (they do not depend on ε_1).

These sum rules can be derived by realizing that when a unit charge is infinitely close to, for example, the $\varepsilon_1|\varepsilon_2$ boundary on the right-hand side ($d/\delta \rightarrow 0$, where d is the distance from the boundary), then the other ($\varepsilon_2|\varepsilon_3$) boundary is infinitely far. Therefore, the simple image charge solution can be used, which provides $\alpha_1(0)$ in eq 7 for the total induced charge (the magnitude of the image charge). This induced charge, however, is also a point charge and sits on top of the source charge, when this source charge is infinitely close to the boundary. The two charges together form a $2q/(\varepsilon_1 + \varepsilon_2)$ effective charge, for which the other ($\varepsilon_2|\varepsilon_3$) boundary is present as a lonely dielectric boundary and the image charge solution can be used again. The solution provides $\alpha_2(0)$ in eq 7. The other limiting values ($\alpha_1(\delta)$, $\alpha_1(\infty)$, $\alpha_2(\delta)$, and $\alpha_2(\infty)$) can be derived similarly. ICC calculations confirmed these results.

Computation of the Energy. The interaction between two hard sphere ions of equal radii, R , can be described by the sum of the hard sphere and the screened Coulomb potential:

$$\left\{ \begin{array}{ll} \infty & \text{if } r < 2R \\ \frac{1}{4\pi\varepsilon_0\varepsilon_3} \frac{q_i q_j}{r} & \text{if } r > 2R \end{array} \right. \quad (9)$$

where r is the distance of the ions, q_i is the charge of ionic species i , and ε_0 is the permittivity of vacuum.

The total surface charge on the $\varepsilon_1|\varepsilon_2$ dielectric boundary containing all surface charges or those induced by them is

$$\sigma'_1 = \frac{\sigma}{\varepsilon_2} + \alpha_1(0)\sigma + \alpha_1(\infty)\sigma_H \quad (10)$$

where the first term, σ/ε_2 , is an effective charge that contains the σ electrode charge (that is in the ε_2 region on the surface of the electrode) and the $(1/\varepsilon_2 - 1)\sigma$ induced charge (that is also a

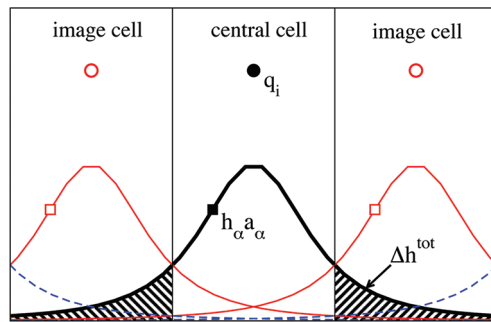


Figure 3. Illustration of the induced charges induced by a source charge (filled circle) in the central simulation cell and by its periodic replicas (open circles). The periodic replicas of the induced charge distribution are shown. Induced charges in the central simulation cell (filled square) are computed by ICC and taken into account explicitly (eq 18). Its periodic images (open squares) are treated by the charged sheet method (eq 19). All the tails outside the finite simulation cells are replaced by an infinite charged sheet (eqs 20 and 21)).

surface charge on top of the electrode charge). The second and third terms are the charges induced by the σ electrode charge and the σ_H charge on the confining wall at $x = H$, respectively, on the first dielectric boundary. The electrostatic interaction of an ion q_i at x_i with the σ'_1 surface charge on the first dielectric boundary is

$$-\frac{q_i \sigma'_1}{4\epsilon_0} x_i \quad (11)$$

The total surface charge on the $\varepsilon_2|\varepsilon_3$ dielectric boundary induced by all the surface charges in the system is

$$\sigma'_2 = \alpha_2(0)\sigma + \alpha_2(\infty)\sigma_H \quad (12)$$

where the first and second terms are the charges induced by the σ electrode charge and the σ_H surface charge, respectively, on the second dielectric boundary. The electrostatic interaction of an ion q_i at x_i with the σ'_2 surface charge on the second dielectric boundary is

$$-\frac{q_i \sigma'_2}{4\epsilon_0} (x_i - \delta) \quad (13)$$

There is an interaction missing from the above equations, the energy of the electrode charge σ with the field of an ionic point charge q_i/ε_3 at x_i :

$$-\frac{\sigma q_i}{4\pi\epsilon_0\varepsilon_3} x_i \quad (14)$$

In this equation, q_i/ε_3 is also an effective charge that contains the ionic charge q_i and the induced charge $(1/\varepsilon_3 - 1)q_i$ superimposed on it.

The interaction energy of an ion with the periodic images outside the central simulation cell can be approximated with the charged sheet method.^{45,46} In this method, the periodic images of a charge q_j at position x_j in the central simulation cell are smeared into a constant surface charge q_j/L^2 . The potential of this holed sheet at position x_i can be given as

$$\phi^{\text{csh}}(q_j, x_j, x_i) = -\frac{1}{2\epsilon_0 L^2} \frac{q_j}{L^2} |x_i - x_j| - \frac{q_j}{L^2} \phi^{\text{hole}}(x_i - x_j, L) \quad (15)$$

where the first term is the potential of the infinite sheet from which we deduct the second term. The second term is the potential of the part of the sheet (the “hole”) in the central

simulation cell: this has to be deducted because we take these interactions into account explicitly. The potential above the center of a $L \times L$ patch (carrying unit surface charge) in a distance $|x|$ from it is

$$\begin{aligned}\phi^{\text{hole}}(x, L) = & -\frac{1}{2\epsilon_0}|x| + \frac{|x|}{\pi\epsilon_0} \arctan \frac{4|x|r_1}{L} \\ & + \frac{L}{\pi\epsilon_0} \ln \left(\frac{0.5 + r_1}{r_2} \right)\end{aligned}\quad (16)$$

where $r_1 = (0.5 + (x/L)^2)^{1/2}$ and $r_2 = (0.25 + (x/L)^2)^{1/2}$. This equation was originally derived by Torrie and Valleau⁴⁵ and later by us⁴⁶ in a slightly different form. The interaction energy of an ion q_i (at position x_i) with the charged sheet of another ion q_j (at position x_j) is

$$q_i \phi^{\text{csh}}(q_j/\epsilon_3, x_j, x_i) \quad (17)$$

The energies associated with the polarization charges induced by the ions can be collected on the basis of Figure 3. A source charge in the central simulation cell (filled circle) induces a surface charge distribution on a dielectric boundary (thick black line). The portion of this distribution in the central simulation cell is computed by ICC and the induced charge h_α for the tile α is treated as a point charge $h_\alpha a_\alpha$ (filled square) placed in the tile center s_α . The interaction energy of an ion q_i at position r_i with this induced charge is then calculated directly as

$$\frac{1}{8\pi\epsilon_0} \frac{q_i h_\alpha a_\alpha}{|\mathbf{r}_i - \mathbf{s}_\alpha|} \quad (18)$$

where $|\mathbf{r}_i - \mathbf{s}_\alpha|$ is also a minimum image distance (just like r in eq 9).

There are, however, periodic images of the source charge in the neighboring image cells (open circles) that also induce the same but shifted charge distributions (thin red lines and blue dashed lines) on the dielectric boundary. The interaction with the periodic images of $h_\alpha a_\alpha$ (open squares) must also be taken into account with the charged sheet method. The interaction energy of an ion q_i with the charged sheet of an induced charge $h_\alpha a_\alpha$ is

$$0.5 \times q_i \phi^{\text{csh}}(h_\alpha a_\alpha, x_\alpha, x_i) \quad (19)$$

where x_α is the x -coordinate of the tile center. Thus, all the charges on the finite dielectric boundaries \mathcal{S}_j and their periodic images have been taken into account. There are, however, the missing charges, Δh_j^{tot} , because only a finite part of the whole infinite dielectric boundary was included in the ICC calculation. These are indicated by the shaded tails in Figure 3. The tails of the periodic replicas of the induced charge, however, appear in every simulation cell (the tail of the thin red line, for example, extends into the central simulation cell). Thus, the Δh_1^{tot} and Δh_2^{tot} correction charges appear in the central simulation cell and in its every replica. Consequently, these charges can be smeared into an infinite charged sheet. The interactions of an ion q_i (at position x_i) with the correction charges Δh_1^{tot} and Δh_2^{tot} then can be computed as

$$-\frac{q_i \Delta h_1^{\text{tot}}}{4\epsilon_0} x_i \quad (20)$$

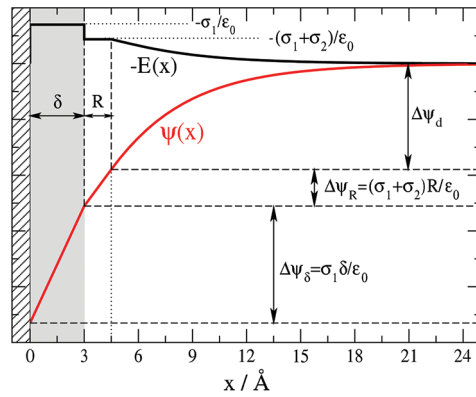


Figure 4. Illustration of electrostatics for a DL near a slab geometry. The profiles $-E(x)$ (black line) and $\psi(x)$ (red line) are shown. The electric field and the potential drop in the inner layer are σ_1/ϵ_0 and $\Delta\psi_\delta = \psi(0) - \psi(\delta) = \sigma_1\delta/\epsilon_0$, respectively (σ_1 is the total (induced and source) charge on the $\epsilon_1|\epsilon_2$ boundary, see eq 23). The electric field and potential drop in the contact layer ($\delta < x < \delta + R$) are $(\sigma_1 + \sigma_2)/\epsilon_0$ and $\Delta\psi_R = \psi(\delta) - \psi(\delta + R) = (\sigma_1 + \sigma_2)R/\epsilon_0$, respectively (σ_2 is the total (induced only) charge on the $\epsilon_2|\epsilon_3$ boundary; see eq 24). The potential drop in the diffuse layer is $\Delta\psi_d$.

and

$$-\frac{q_i \Delta h_2^{\text{tot}}}{4\epsilon_0} (x_i - \delta) \quad (21)$$

Monte Carlo Simulations. The system outlined in the previous subsections has been simulated with MC simulations in the canonical ensemble. In this ensemble, the volume V , the temperature T , and the numbers of the ions of the different species N_i are fixed. The number of particles was chosen to obtain about 0.5 M concentration in the middle of the simulation cell. The concentration that we obtained as the result of the simulation is a little larger than the targeted 0.5 M. The small deviation does not influence our conclusions. In our figures, we will plot the density profiles $g_i(x) = \rho_i(x)/\rho_+^b$ normalized by the bulk density of the cation. The density profiles $\rho_i(x)$ are obtained as a direct result of the simulation, while ρ_+^b is the average of the profile for the middle of the cell, where the $\rho_i(x)$ profile is constant.

Ion displacement steps were applied in the Metropolis sampling scheme.^{47,48} The dimension L of the simulation cell was large enough so that using a larger value did not influence our results ($L = 70$ Å is a typical value). The dimension H of the simulation cell was large enough so that a decent bulk region was formed in the middle of the cell ($H = 140$ Å is a typical value). The number of ions (200 is a typical value) and cell dimensions were chosen to target 0.5 M concentration. The number of sampled configurations was large enough to obtain smooth profiles (2×10^8 is a typical value).

We placed surface charge $\sigma_H = -\sigma$ on the confining wall at $x = H$. In this way, the number of ions and σ could be chosen independently. The numbers of ions were fixed to provide a charge neutral system without any restriction from the value of σ .

The \mathcal{S}_i dielectric boundaries were divided into squares of size $\Delta y \times \Delta y$, with a typical value for $\Delta y \approx 3$ Å. A typical value for the number of tiles was 1152. A detailed analysis of the effect of Δy on the accuracy of simulation results was given in ref 42.

Calculation of the Electric Field and Potential Profiles. The results of the simulations are the density profiles $\rho_i(x)$. From the

density profiles the charge profile is calculated as

$$q(x) = \sum_i z_i e \rho_i(x) \quad (22)$$

To solve Poisson's equation, we need the total charges on the $\varepsilon_1|\varepsilon_2$ and $\varepsilon_2|\varepsilon_3$ boundaries. These charges can be obtained from the sum rules (eqs 7 and 8). The total surface charge on the $\varepsilon_1|\varepsilon_2$ dielectric boundary is

$$\sigma_1 = \frac{\sigma}{\varepsilon_2} + \alpha_1(0)\sigma + \alpha_1(\infty)(-\sigma) \quad (23)$$

where the first and second terms also appeared in eq 10. If we assume that the σ_H is perfectly balanced by the ions in the DL near it (the DLs at $x = 0$ and $x = H$ are independent: the cell is long enough), they do not appear in σ_1 . The charge in the diffuse layer at $x = 0$, on the other hand, is present (it did not appear in eq 10, because the interactions with these charges were computed explicitly). The magnitude of the diffuse layer charge is the opposite of the electrode charge ($-\sigma$) due to the requirement of charge neutrality.

$$\psi(x) = \begin{cases} -\frac{\sigma_1}{\varepsilon_0}x + C & \text{if } 0 < x < \delta \\ -\frac{\sigma_1}{\varepsilon_0}\delta - \frac{\sigma_1 + \sigma_2}{\varepsilon_0}(x - \delta) + C & \text{if } \delta < x < \delta + R \\ -\frac{\sigma_1}{\varepsilon_0}\delta - \frac{\sigma_1 + \sigma_2}{\varepsilon_0}(x - \delta) - \frac{1}{\varepsilon_0} \int_{\delta+R}^x \left[\int_{\delta+R}^{x'} q(x'') dx'' \right] dx' + C & \text{if } \delta + R < x \end{cases}$$

The integration constant in eq 25 is zero and is set by the Neumann boundary condition that the normal electric field is zero outside the simulation cell ($x < 0$). The integration constant C in eq 26 can be chosen arbitrarily. Here, we set the zero level of the potential to the central bulk region of the cell.

The $-E(x)$ and $\psi(x)$ functions are illustrated in Figure 4 for a typical situation (a 1:1 electrolyte with a negative σ). The potential drops in the three relevant regions are shown in the figure:

- $\Delta\psi_\delta = \sigma_1\delta/\varepsilon_0 = 2\sigma\delta/[\varepsilon_0(\varepsilon_2 + \varepsilon_3)]$ in the inner layer, $0 < x < \delta$,
- $\Delta\psi_R = [(\sigma_1 + \sigma_2)R]/\varepsilon_0 = \sigma R/\varepsilon_0\varepsilon_3$ in the layer between the $\varepsilon_2|\varepsilon_3$ boundary and the DCA plane of the ions ($\delta < x < \delta + R$, we will call this layer the contact layer from now), and
- $\Delta\psi_d$ in the diffuse layer, $\delta + R < x$.

The electric field in the first two layers is constant, and the potential is linear. The electric fields in these layers (and also the slopes of the potential) can be different because the plane at $x = \delta$ can carry induced charges (σ_2) if that plane is a dielectric boundary ($\varepsilon_2 \neq \varepsilon_3$).

RESULTS AND DISCUSSION

In this study, we fix the values $\varepsilon_1 \rightarrow \infty$, $\varepsilon_3 = 80$, $\delta = 3 \text{ \AA}$, $R = 1.5 \text{ \AA}$, and $T = 298.15 \text{ K}$. In the simulations, we changed either the value of the inner layer dielectric constant ε_2 or the electrode charge σ . We performed simulations for 1:1 and 2:1 RPM electrolytes.

Changing Electrode Charge. First, we fixed the inner layer dielectric constant at $\varepsilon_2 = 6$ (the value used in our previous study²⁹) and changed the electrode charge σ . Figures 5 and 6 show the profiles for 1:1 and 2:1 electrolytes, respectively.

Similarly, the total surface charge on the $\varepsilon_2|\varepsilon_3$ dielectric boundary is

$$\sigma_2 = \alpha_2(0)\sigma + \alpha_2(\infty)(-\sigma) \quad (24)$$

where, again, the diffuse layer $-\sigma$ charge appears instead of σ_H .

To compute the electric field and potential profiles from the charge profile $q(x)$ and the surface charges σ_1 and σ_2 , Poisson's equation has to be solved with appropriate boundary conditions. Here we use a method (developed recently), in which Neumann boundary conditions are used. The resulting equations are

$$E(x) = \begin{cases} \frac{\sigma_1}{\varepsilon_0} & \text{if } 0 < x < \delta \\ \frac{\sigma_1 + \sigma_2}{\varepsilon_0} & \text{if } \delta < x < \delta + R \\ \frac{\sigma_1 + \sigma_2}{\varepsilon_0} + \frac{1}{\varepsilon_0} \int_{\delta+R}^x q(x') dx' & \text{if } \delta + R < x \end{cases} \quad (25)$$

and

$$\psi(x) = \begin{cases} -\frac{\sigma_1}{\varepsilon_0}x + C & \text{if } 0 < x < \delta \\ -\frac{\sigma_1}{\varepsilon_0}\delta - \frac{\sigma_1 + \sigma_2}{\varepsilon_0}(x - \delta) + C & \text{if } \delta < x < \delta + R \\ -\frac{\sigma_1}{\varepsilon_0}\delta - \frac{\sigma_1 + \sigma_2}{\varepsilon_0}(x - \delta) - \frac{1}{\varepsilon_0} \int_{\delta+R}^x \left[\int_{\delta+R}^{x'} q(x'') dx'' \right] dx' + C & \text{if } \delta + R < x \end{cases} \quad (26)$$

Figure 5 shows the profiles only for negative electrode charges because the behavior is the same at positive electrode charges due to symmetry (cations and anions have the same radii). The normalized density $g_i(x)$ and the charge profiles $q(x)$ are provided by the simulations, while the electric field and potential profiles are computed from eqs 25 and 26.

The $g_i(x)$ density profiles decrease near the inner layer for zero electrode charge. This behavior was already found in our earlier work.²⁹ This phenomenon is well-known for DLs near polarizable electrodes with repulsive image charges when $\varepsilon_1 = 1$ (in the absence of the ε_2 layer).^{12–14,18,19,27,49} The conclusion is that the presence of a finite-thickness dielectric inner layer (near an $\varepsilon_1 \rightarrow \infty$ electrode) has similar effect on the density profiles as if the low dielectric layer would extend to $-\infty$ (e.g., $\varepsilon_1 = \varepsilon_2$). A nonzero positive (negative) electrode charge works against this depletion effect for anions (cations).

The electric fields are constant in the inner and contact layers because they are proportional to the constant surface charges σ_1 and $\sigma_1 + \sigma_2$, respectively. The electric fields in these layers are different because the polarization charge induced on the $\varepsilon_2|\varepsilon_3$ boundary (σ_2) is nonzero. Accordingly, the potential profiles have different slopes in these layers.

In the case of the 2:1 system, the cation profiles have an interesting behavior at large negative electrode charge (Figure 6). They show an increasing tendency approaching the electrode from bulk because of the attractive electrode charge, while, after a maximum, they show a depletion near the inner layer due to the repulsion of the induced charges on the $\varepsilon_2|\varepsilon_3$ boundary. The nonmonotonic behavior is a consequence of the different ranges of the electrostatic forces of the two kinds of charges. The electrode

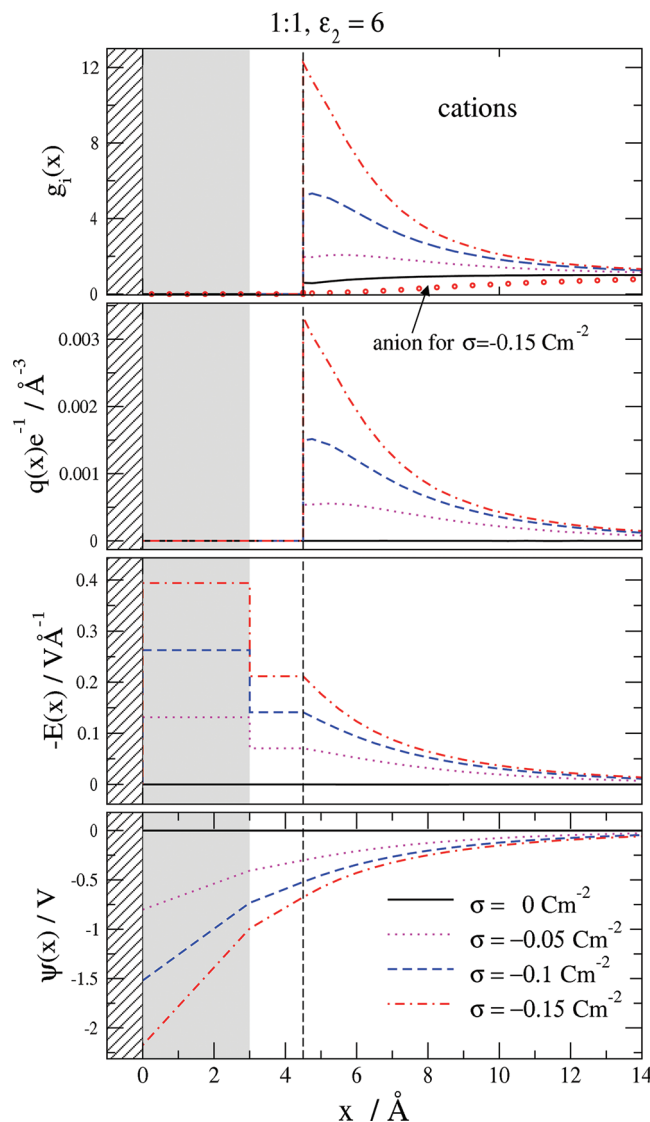


Figure 5. Normalized density, charge, electric field, and potential profiles for the DL of a 1:1 electrolyte formed near a $\epsilon_2 = 6$ inner layer for different electrode charges. The anion profiles are indistinguishable on the scale of the figure, therefore, only the curve for $\sigma = 0.15 \text{ Cm}^{-2}$ is plotted.

charge and the polarization charges induced by it on the dielectric boundaries are infinite surface charges with a long-range effect (see eqs 11 and 13). The interaction with the instantaneously induced charges on the dielectric boundaries, however, has a $1/r$ distance dependence (see eq 18). The dominant term that causes the depletion of the divalent cations is the repulsion of the polarization charge induced by the cation itself approaching the $\epsilon_2|\epsilon_3$ boundary. This behavior is absent in the case of the monovalent anions. The 4 times larger repulsion in the case of divalent ions is necessary to produce this effect. Because the cation profiles dominate the charge profiles at large negative electrode charges, this behavior can be observed in the charge profiles as well.

The charge profile of the 2:1 system at zero electrode charge shows the well-known behavior that it is not zero due to the charge asymmetry of the cation and the anion.⁵⁰ Consequently, the electric field profile is not zero in the diffuse layer, although it is zero in the inner and contact layers. The potential, therefore, has a nonzero value at zero electrode charge (PZC), although it

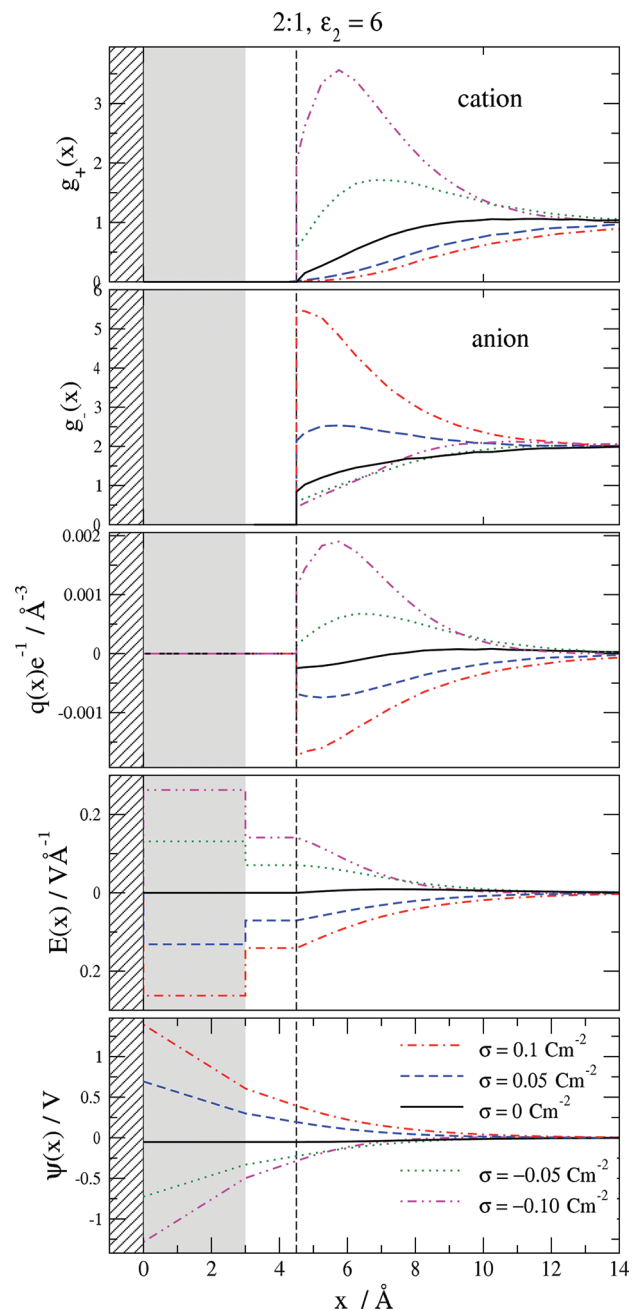


Figure 6. Normalized density, charge, electric field, and potential profiles for the DL of a 2:1 electrolyte formed near a $\epsilon_2 = 6$ inner layer for different electrode charges. The anion profiles are normalized by the bulk concentration of the cation.

cannot be observed in Figure 6 due to the scale of the ordinate (its value is about -0.05 V).

Figure 7 summarizes the potential vs electrode charge relationships depicted from Figure 5 and Figure 6. It shows the $\Delta\psi_\delta$, $\Delta\psi_R$, and $\Delta\psi_d$ values illustrated in Figure 4. The potential drops $\Delta\psi_\delta$ and $\Delta\psi_R$ are linear functions of σ . The diffuse layer potential $\Delta\psi_d$ has the well-known nonlinear behavior (discussed in ref 51, for example). At this value of ϵ_2 , the dominant term is the inner layer potential $\Delta\psi_\delta$.

This term is large in our model because the inner layer is an ion-free region. We expect that simulations for a model where ions can enter the inner layer will provide smaller $\Delta\psi_\delta$ values.

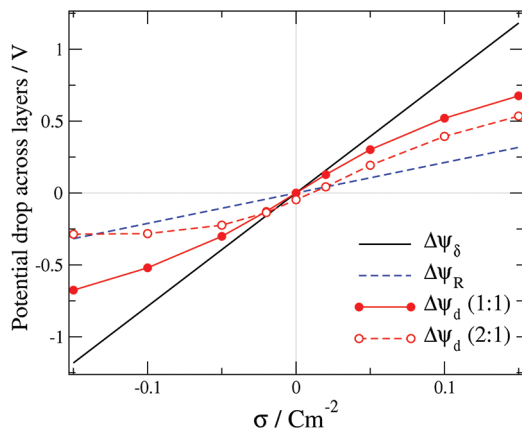


Figure 7. The potential drops across the inner layer ($\Delta\psi_\delta$), the contact layer ($\Delta\psi_R$), and the diffuse layer ($\Delta\psi_d$) as functions of the electrode charge for a DL formed near an $\epsilon_2 = 6$ inner layer. The diffuse layer potential drop is different for the 1:1 and the 2:1 cases, while the $\Delta\psi_\delta$ and $\Delta\psi_R$ values are independent of the properties of the diffuse layer: they are identical for the 1:1 and 2:1 cases.

Changing the Inner Layer Dielectric Constant. Next, we fixed the electrode charge ($\sigma = \pm 0.02 \text{ Cm}^{-2}$) and changed the inner layer dielectric constant between the values $\epsilon_2 = 6$ and 80. Figure 8 shows the profiles for a 1:1 electrolyte for $\sigma = -0.02 \text{ Cm}^{-2}$. The profiles for a 2:1 electrolyte in the case of a positive ($\sigma = 0.02 \text{ Cm}^{-2}$) and a negative ($\sigma = -0.02 \text{ Cm}^{-2}$) electrode charge are shown in Figure 9 and Figure 10, respectively. In these figures, the anion concentration profiles are normalized by the cation bulk concentration (so their bulk limit is 2) in order to make cation and anion profiles distinguishable.

The common behavior of all the $g(x)$ density profiles in Figures 8–10 is that they decrease near the inner layer as the dielectric constant of the inner layer (ϵ_2) decreases. The profiles of the co-ion and the counterion are influenced differently by the value of ϵ_2 . In the 1:1 case, the cation (counterion) profiles are affected more than the anion (co-ion) profiles. The explanation is probably that the co-ion profiles are already depleted, so there is no room for extra depletion due to the decrease of ϵ_2 . The charge profile changes accordingly: it decreases near the inner layer with ϵ_2 , which is balanced by an increase in the diffuse layer farther from the electrode. This balance is necessary because the integral of the charge profile is fixed because the electrode charge is fixed. Changing ϵ_2 does not change this fact. Taking the induced charges into account, the integral of all the effective q_i/ϵ_3 charges must balance all the charges on the dielectric boundaries: $\sigma_1 + \sigma_2 = \sigma/\epsilon_3$. This value is independent of ϵ_2 too, as shown by the constant electric field in the contact layer ($\delta < x < \delta + R$).

The value of ϵ_2 , however, influences the electric field in the inner layer ($0 < x < \delta$); its magnitude increases as ϵ_2 decreases. This is because the surface charge on the electrode - inner layer boundary, σ_1 , changes with ϵ_2 . This change is shown in Figure 11. The top panel shows the components of the σ_1 charge. It is seen that the σ/ϵ_2 electrode charge (black dashed line) and the charge induced by it on the $\epsilon_1|\epsilon_2$ boundary (red dot-dashed line), $\alpha_1(0)\sigma$, are equal in magnitude and opposite in sign (see the value of $\alpha_1(0)$ in eq 8). Any charge infinitely close to the metal electrode induces its opposite on the surface of the electrode. The two charges cancel each other, because they are on top of each other. The charge that contributes to σ_1 is the charge induced by the ionic charges in the diffuse layer, $\alpha_1(\infty)(-\sigma)$, (blue solid line).

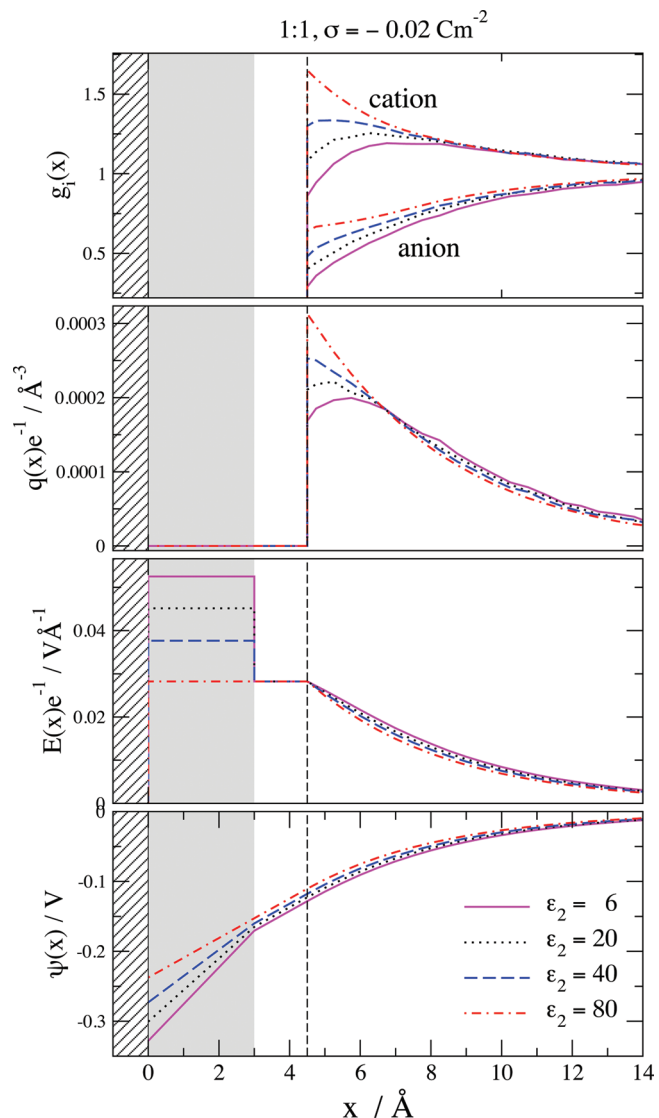


Figure 8. Normalized density, charge, electric field, and potential profiles for the DL of a 1:1 electrolyte formed near a ϵ_2 inner layer for electrode charge $\sigma = -0.02 \text{ Cm}^{-2}$ for different values of ϵ_2 .

The bottom panel of Figure 11 shows the components of σ_2 . There is no source charge on this dielectric boundary, so any charge on it is either induced by the electrode charge (σ at $x = 0$) or the diffuse layer charge ($-\sigma$ in the region $x > \delta + R$). According to the sum rule, the former term is zero (see the value of $\alpha_2(0)$ in eq 8). Therefore, σ_2 also consists of the polarization charge induced by the ions in the diffuse layer ($\alpha_2(\infty)(-\sigma)$).

The bottom panel of Figure 11 also shows σ_1 , σ_2 , and their sum. It is seen that σ_1 and σ_2 has the same ϵ_2 -dependence, but with opposite signs. Their sum is constant with the value σ/ϵ_3 . The behavior of the σ_1 and σ_2 charges, as well as the electric fields in the inner and contact layers (that are associated with these charges; see eq 25) results in a linear behavior of the electric potential with different slopes in the inner and contact layers (bottom panels of Figures 8–10).

The fact that the value of ϵ_2 has different effects on the counterions and the co-ions has its consequences on the charge, field, and potential profiles too. The value of ϵ_2 also influences the behavior of the electric field in the diffuse layer: the field declines

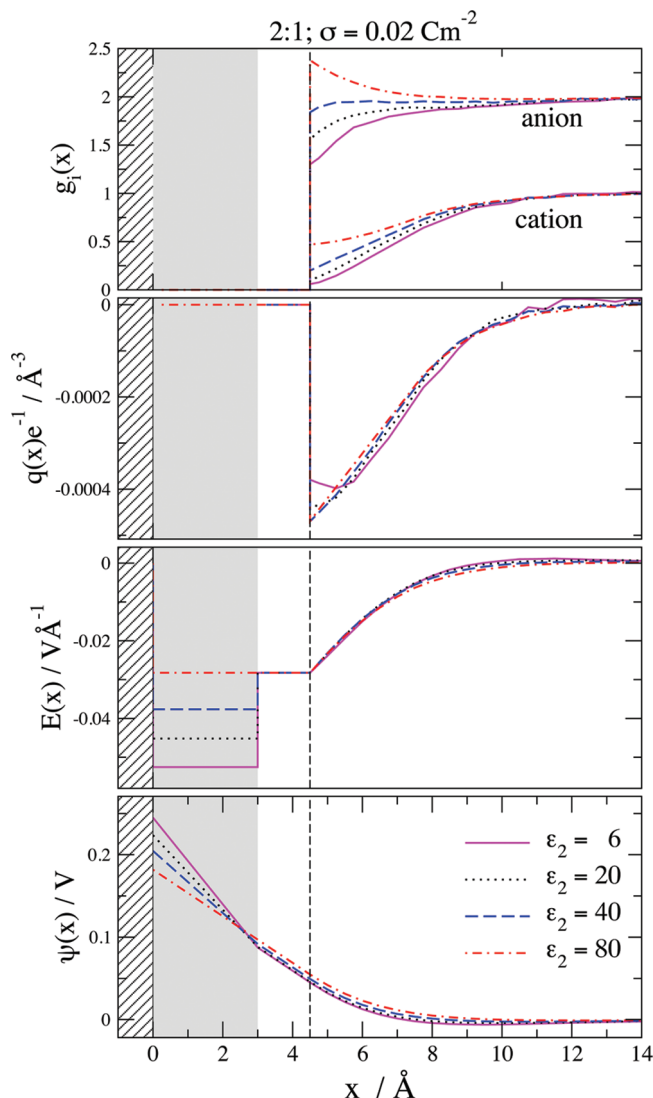


Figure 9. Normalized density, charge, electric field, and potential profiles for the DL of a 2:1 electrolyte formed near a ϵ_2 inner layer for electrode charge $\sigma = 0.02 \text{ Cm}^{-2}$ for different values of ϵ_2 . The anion profiles are normalized by the bulk concentration of the cation.

to zero at a smaller rate for lower ϵ_2 . This change in the behavior of $E(x)$ results in a different behavior of the potential profiles, therefore, in a different diffuse layer potential, $\Delta\psi_d$. The presence of the low dielectric inner layer has a clear effect on $\Delta\psi_d$ although this effect is small for the 1:1 system shown in Figure 8.

The behavior of the curves for the 2:1 system is quite similar to that of the 1:1 system for positive electrode charge, namely, when the monovalent anion is the counterion (Figure 9). The behavior of the 2:1 system for negative electrode charge, however, has a very strong ϵ_2 -dependence (Figure 10). The different effects of the electrode charge and the instantaneous polarization charge induced by ions (discussed above) has a distinctive effect in the case of divalent ions being the counterions. In this case, the attractive effect of the electrode charge and the repulsive effect of the instantaneous induced charges have a strong competition. The strength of this competition depends on the value of ϵ_2 . The result is a strong ϵ_2 -dependence of the charge, field, and potential profiles in the diffuse layer. (The ϵ_2 -dependence of these profiles

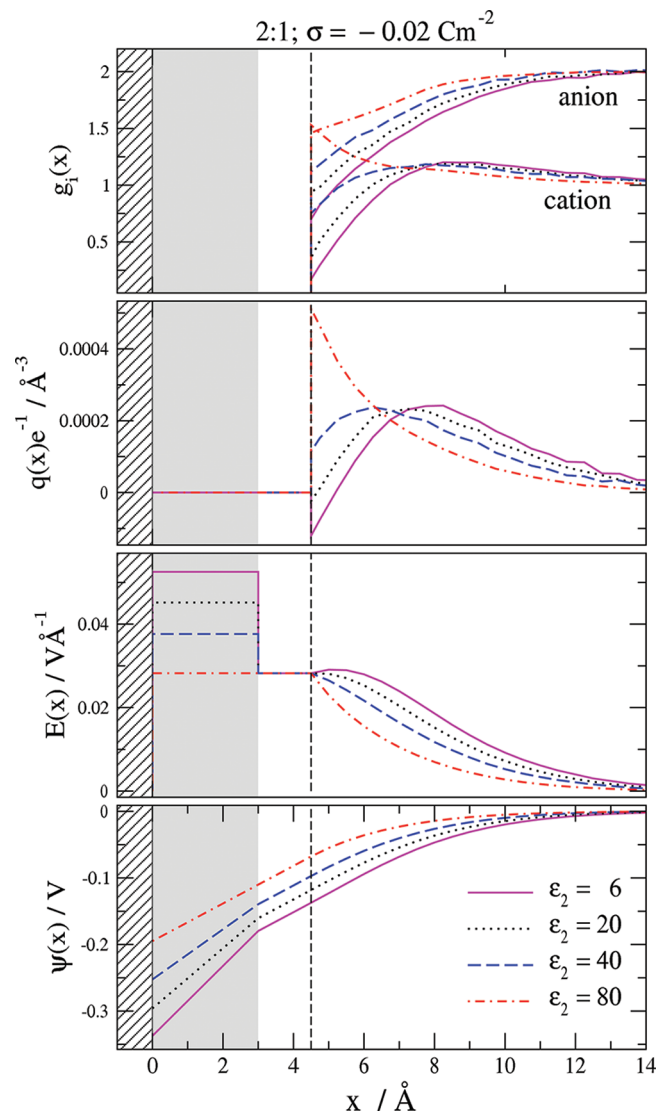


Figure 10. Normalized density, charge, electric field, and potential profiles for the DL of a 2:1 electrolyte formed near a ϵ_2 inner layer for electrode charge $\sigma = -0.02 \text{ Cm}^{-2}$ for different values of ϵ_2 . The anion profiles are normalized by the bulk concentration of the cation.

in the inner and contact layers is the same as for positive electrode charge, but with the opposite sign.)

The fact that the value of ϵ_2 influences the behavior of the diffuse layer has its consequences on the capacitance. We can write the inverse capacitance as a sum of three terms:

$$\frac{1}{C} = \frac{1}{C_\delta} + \frac{1}{C_R} + \frac{1}{C_d} \quad (27)$$

where C_δ , C_R , and C_d are the capacitances of the inner, the contact, and the diffuse layer, respectively. These capacitances are associated with the potential drops $\Delta\psi_\delta$, $\Delta\psi_R$, and $\Delta\psi_d$ defined before. Figure 12 shows these terms as functions of the inner layer dielectric constant for the 1:1 and 2:1 electrolytes studied. The inner layer capacitance is

$$C_\delta = \frac{\sigma}{\Delta\psi_\delta} = \frac{\sigma}{\sigma_1 \delta / \epsilon_0} = \epsilon_0 \frac{\epsilon_2 + \epsilon_3}{2\delta} \quad (28)$$

where eq 23 was used for σ_1 .

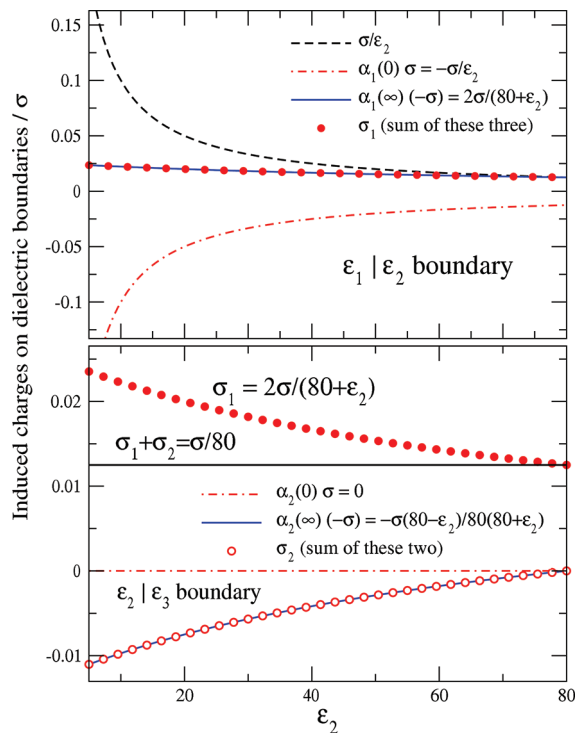


Figure 11. The polarization charges induced on the $\epsilon_1|\epsilon_2$ and $\epsilon_2|\epsilon_3$ boundaries by the σ electrode charge. The components of the total surface charges, σ_1 and σ_2 , on these boundaries are shown. The figure shows the values for $\epsilon_1 \rightarrow \infty$ and $\epsilon_3 = 80$ as functions of ϵ_2 .

This equation has a different ϵ_2 -dependence than the traditional result $C_\delta = \epsilon_0\epsilon_2/\delta$. This ϵ_2 -dependence can be recovered in two ways. (1) In the case of a metal electrode ($\epsilon_1 \rightarrow \infty$), the $C_\delta = \epsilon_0\epsilon_2/\delta$ result is recovered if $\epsilon_2 = \epsilon_3$. In this case, however, we do not have the low-dielectric inner layer. (2) In the general case (ϵ_1 is finite), the total charge on the electrode is

$$\sigma_1 = \frac{2(\epsilon_1 + \epsilon_3)}{(\epsilon_1 + \epsilon_2)(\epsilon_2 + \epsilon_3)} \sigma \quad (29)$$

The $C_\delta = \epsilon_0\epsilon_2/\delta$ result is recovered if $\epsilon_1 = \epsilon_2$. In this case, however, we do not have a metal electrode. Instead, we have an electrode whose dielectric constant is equal to that of the inner layer.

The contact layer capacitance depends only on the ionic radius and ϵ_3 :

$$C_R = \frac{\sigma}{\Delta\psi_R} = \epsilon_0 \frac{\sigma}{(\sigma_1 + \sigma_2)R} = \epsilon_0 \frac{\epsilon_3}{R} \quad (30)$$

As a matter of fact, this quantity is not well-defined: in the case of ions of different sizes (or different DCAs), it must be defined with the DCA plane of the smallest ion. The best solution probably is to merge it into C_d .

The diffuse layer capacitance, as opposed to the common assumption of PB theories, depends on the value of ϵ_2 . The mechanism described before (the interface acts differently on co-ions and counterions) makes the behavior of ions in the diffuse layer different for different values of ϵ_2 .

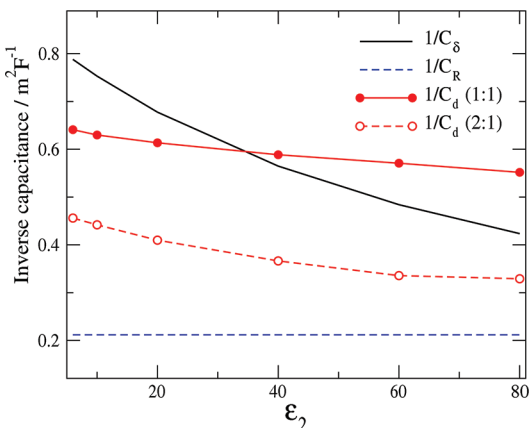


Figure 12. The terms of the inverse capacitance associated with the inner layer (C_δ^{-1}), the contact layer (C_R^{-1}), and the diffuse layer (C_d^{-1}) as functions of the inner layer dielectric constant.

SUMMARY

We have studied the behavior of a DL formed near a low dielectric inner layer that is a dielectric slab between a perfectly polarizable electrode ($\epsilon_1 \rightarrow \infty$) and the diffuse layer (ϵ_3). We have examined both (1) the induced charges on the two dielectric boundaries and (2) the diffuse layer formed by the ions.

(1) Sum rules provided the induced charges on the surface of the electrode (σ_1) and on the boundary of the inner layer and the diffuse layer (σ_2). We have found that the slope of the potential in the inner layer, and, therefore, the inner layer capacitance, depends on $(\epsilon_2 + \epsilon_3)/2$ instead of ϵ_2 as traditional theoretical considerations assume as in the solution of Andreu et al.,⁹ for example. The $C_\delta = \epsilon_0\epsilon_2/\delta$ result is obtained if we assume that the total charge on the electrode is σ/ϵ_2 . This assumption ignores the induced charges $\alpha_1(0)\sigma$ and $\alpha_1(\infty)(-\sigma)$ (see eq 23). These induced charges, however, must be included in the solution of Poisson's equation (see eqs 25 and 26). This result cannot be obtained without using the sum rule to account for all induced charges in the system properly.

Separation of the capacitance into a long-range part (the diffuse layer) and a short-range part (the inner layer) is an artificial assumption. Its validity, however, is well justified by the correct slope of the Parsons-Zobel plot at low concentrations. The nature of the short-term part can be examined by well-defined molecular models associated with statistical mechanical methods with which we study these models. Although the model used in this work is really a simple representation of the inner layer, the MC results revealed a behavior that is different from assumed so far. Our results indicate that interpretation of experimental data with a fitted ϵ_2 dielectric constant of the inner layer must be done using a different equation. Even more intricate behavior is expected from the case, when ions can enter the inner layer.

(2) We have shown that the structure of the DL in the diffuse layer depends on the dielectric constant of the inner layer. This is because the repulsive image charges repel both the counterions and the co-ions, while the electrode charge attracts the counterions and repels the co-ions. The induced charge cannot deplete the co-ions (they are already depleted) the same way as it can deplete the counterions (there is an excess of these ions due to the electrode charge). This produces an asymmetric effect, which obviously depends on the value of ϵ_2 : the effect of induced

charges is stronger for lower ε_2 . This result cannot be obtained without computing the full, many-body effect of induced charges. This is not possible with mean field theories.

The concept of an inner layer that describes the response of the solvent to the electrode charge is an approximation that results from the neglect of the explicit presence of the solvent molecules. In reality, the region in which the solvent molecules respond to the electrode charge must be as thick as the diffuse layer. It is the charge of the ions in the diffuse layer that screens the field of the electrode. As long as the unscreened portion of the electrode field has not vanished, the solvent molecules will respond to the electrode, primarily by orientation. As a result, the solvent interfacial region must be as thick as the diffuse layer. However, we are a long way from having a method of treating the contribution of the solvent molecules that is useful for experimental analysis. The purpose of this paper is not to dismiss the deficiencies of the inner layer concept but to proceed step by step and provide a more useful method of using this concept by fitting ε_2 to experimental data.

AUTHOR INFORMATION

Corresponding Author

*E-mail: boda@almos.vein.hu.

ACKNOWLEDGMENT

These simulations were made possible by a generous allotment of computer time by the Ira and Mary Lou Fulton supercomputer facility at Brigham Young University. This is acknowledged with thanks. The work was supported by the Hungarian National Research Fund (OTKA K75132).

REFERENCES

- (1) Gouy, G. *J. Phys. (Paris)* **1910**, *9*, 457–468.
- (2) Chapman, D. L. *Philos. Mag.* **1913**, *25*, 475–481.
- (3) Blum, L. *J. Phys. Chem.* **1977**, *81*, 136–147.
- (4) Outhwaite, C. W.; Bhuiyan, L. B. *J. Chem. Soc., Faraday Trans. 1983*, *79*, 707–718.
- (5) Plischke, M.; Henderson, D. *J. Chem. Phys.* **1988**, *88*, 2712–2718.
- (6) Plischke, M.; Henderson, D. *J. Chem. Phys.* **1989**, *90*, 5738–5741.
- (7) Mier y Teran, L.; Suh, S.; White, H. S.; Davis, H. *J. Chem. Phys.* **1990**, *92*, 5087–5098.
- (8) Valleau, J. P.; Torrie, G. M. *J. Chem. Phys.* **1982**, *76*, 4623–4630.
- (9) Andreu, R.; Molero, M.; Calvente, J.; Carbajo, J. *J. Electroanal. Chem.* **1993**, *358*, 49–62.
- (10) Bhuiyan, L. B.; Blum, L.; Henderson, D. *J. Chem. Phys.* **1983**, *78*, 442–445.
- (11) Spitzer, J. *J. Colloid Interface Sci.* **1983**, *92*, 198–203.
- (12) Croxton, T.; D. A. M.; Patey, G. N.; Torrie, G. M.; Valleau, J. P. *Can. J. Chem.* **1981**, *59*, 1998–2003.
- (13) Torrie, G. M.; Valleau, J. P.; Patey, G. N. *J. Chem. Phys.* **1982**, *76*, 4615–4622.
- (14) Torrie, G. M.; Valleau, J. P.; Outhwaite, C. W. *J. Chem. Phys.* **1984**, *81*, 6296–6300.
- (15) Bratko, D.; Jönsson, B.; Wennerström, H. *Chem. Phys. Lett.* **1986**, *128*, 449–454.
- (16) Linse, P. *J. Phys. Chem.* **1986**, *90*, 6821–6828.
- (17) Messina, R. *J. Chem. Phys.* **2002**, *117*, 11062–11074.
- (18) Bhuiyan, L. B.; Outhwaite, C. W.; Henderson, D.; Alawneh, M. *Mol. Phys.* **2007**, *105*, 1395–1402.
- (19) Alawneh, M.; Henderson, D. *Mol. Simul.* **2007**, *33*, 541–547.
- (20) Alawneh, M.; Henderson, D.; Outhwaite, C. W.; Bhuiyan, L. B. *Mol. Simul.* **2008**, *34*, 501–507.
- (21) Hatlo, M. M.; Lue, L. *Soft Matter* **2008**, *4*, 1582–1596.
- (22) Reščić, J.; Linse, P. *J. Chem. Phys.* **2008**, *129*, 114505.
- (23) Wang, Z. Y.; Ma, Y. Q. *J. Chem. Phys.* **2009**, *131*, 244715.
- (24) Wang, Z. Y.; Ma, Y. Q. *J. Phys. Chem. B* **2010**, *114*, 13386–13392.
- (25) Carnie, S. L.; Chan, D. Y. C. *Mol. Phys.* **1984**, *51*, 1047–1070.
- (26) Kjellander, R.; Marčelja, S. *J. Chem. Phys.* **1985**, *82*, 2122–2135.
- (27) Vertenstein, M.; Ronis, D. *J. Chem. Phys.* **1987**, *87*, 4132–4146.
- (28) Attard, P.; Mitchell, D. J.; Ninham, B. W. *J. Chem. Phys.* **1988**, *89*, 4358–4367.
- (29) Henderson, D.; Gillespie, D.; Nagy, T.; Boda, D. *Mol. Phys.* **2005**, *103*, 2851–2861.
- (30) Wernersson, E.; Kjellander, R. *J. Chem. Phys.* **2006**, *125*, 154702.
- (31) Wernersson, E.; Kjellander, R. *J. Phys. Chem. B* **2007**, *111*, 14279–14284.
- (32) Outhwaite, C.; Bhuiyan, L. *J. Electroanal. Chem.* **2007**, *609*, 51–53.
- (33) Jho, Y. S.; Park, G.; Chang, C. S.; Pincus, P. A.; Kim, M. W. *Phys. Rev. E* **2007**, *76*, 011920.
- (34) Jho, Y. S.; Kanduč, M.; Naji, A.; Podgornik, R.; Kim, M. W.; Pincus, P. A. *Phys. Rev. Lett.* **2008**, *101*, 188101.
- (35) Onsager, L.; Samaras, N. N. T. *J. Chem. Phys.* **1934**, *2*, 528–536.
- (36) Gillespie, D. *J. Phys. Chem. Lett.* **2011**, *2*, 1178–1182.
- (37) Grahame, D. C.; Parsons, R. *J. Am. Chem. Soc.* **1961**, *83*, 1291–1296.
- (38) Parsons, R.; Zobel, F. *J. Electroanal. Chem.* **1965**, *9*, 333–348.
- (39) Valette, G. *J. Electroanal. Chem.* **1981**, *122*, 285–297.
- (40) Valette, G. *J. Electroanal. Chem.* **1982**, *138*, 37–54.
- (41) Parsons, R. *Chem. Rev.* **1990**, *90*, 813–826.
- (42) Boda, D.; Gillespie, D.; Nonner, W.; Henderson, D.; Eisenberg, B. *Phys. Rev. E* **2004**, *69*, 046702.
- (43) Boda, D.; Valiskó, M.; Eisenberg, B.; Nonner, W.; Henderson, D.; Gillespie, D. *J. Chem. Phys.* **2006**, *125*, 034901.
- (44) Boda, D.; Henderson, D.; Eisenberg, B.; Gillespie, D. *J. Chem. Phys.* **2011**, *135*, 064105.
- (45) Torrie, G. M.; Valleau, J. P. *J. Chem. Phys.* **1980**, *73*, 5807–5816.
- (46) Boda, D.; Chan, K. Y.; Henderson, D. *J. Chem. Phys.* **1998**, *109*, 7362–7371.
- (47) Allen, M. P.; Tildesley, D. J. *Computer Simulation of Liquids*; Oxford: New York, 1987.
- (48) Frenkel, D.; Smit, B. *Understanding Molecular Simulations*; Academic Press: San Diego, CA, 1996.
- (49) Nagy, T.; Valiskó, M.; Henderson, D.; Boda, D. *J. Chem. Eng. Data* **2011**, *56*, 1316–1322.
- (50) Valiskó, M.; Henderson, D.; Boda, D. *J. Phys. Chem. B* **2004**, *108*, 16548–16555.
- (51) Boda, D.; Fawcett, W. R.; Henderson, D.; Sokołowski, S. *J. Chem. Phys.* **2002**, *116*, 7170–7176.